

Emission and theoretical studies of Schiff-base [2+2] macrocycles derived from 2,2'-oxydianiline and zinc complexes thereof.

Kuiyuan Wang,^a Kai Chen,^b Tiezheng Bian,^c Yimin Chao,^c Takehiko Yamato,^d Feng Xing,^e Timothy J.

Prior,^a and Carl Redshaw^{a*}

^a *Department of Chemistry, University of Hull, Hull, HU6 7RX, U.K.*

^b *Collaborative Innovation Center of Atmospheric Environment and Equipment Technology, Jiangsu Key Laboratory of Atmospheric Environment Monitoring and Pollution Control, School of Environmental Science and Engineering, Nanjing University of Information Science & Technology, Nanjing 210044, P. R. China.*

^c *School of Chemistry, University of East Anglia, Norwich, NR4 7TJ, U.K.*

^d *Department of Applied Chemistry, Faculty of Science and Engineering, Saga University, Honjo-machi 1, Saga 840-8502, Japan.*

^e *School of Materials and Energy, Guangdong University of Technology, Guangzhou, Guangdong 510006, People's Republic of China.*

Abstract: The emission properties of a number of solvates of the [2+2] Schiff-base macrocycles $\{[2-(\text{OH})-5-(\text{R})-\text{C}_6\text{H}_2-1,3-(\text{CH}_2)_2[\text{O}(2-\text{C}_6\text{H}_4\text{N})_2]]_2$ (R = Me L^1H_2 , *t*Bu L^2H_2 , Cl L^3H_2), formed by reacting 2,6-dicarboxy-4-R-phenol with 2,2'-oxydianiline (2-aminophenylether), $(2-\text{NH}_2\text{C}_6\text{H}_4)_2\text{O}$, have been investigated. Macrocycles L^{1-3}H_2 exhibited different maximum emission wavelengths in different solvents, from λ_{max} at 508 nm (in acetonitrile) to 585 nm (in dichloromethane). DFT studies on systems L^{1-3}H_2 involving solvents of different polarity (DMF *versus* *n*-hexane) indicated that the energy level gap increases with solvent polarity in line with the observed hypochromic shifts. Reaction of

macrocycle L^1H_2 with three equivalents of $ZnBr_2$, in the presence of Et_3N , affords the complex $[(ZnBr)(ZnNCMe)L^1]_2[ZnBr_4] \cdot 2.5MeCN$ (**1**·2.5MeCN). In the case of L^2H_2 , reaction with two equivalents of $ZnBr_2$ affords $[(ZnBr)L^2H_2][ZnBr_3NCMe] \cdot 3MeCN$ (**2**·3MeCN), whilst in the presence of two equivalents of Et_3N , work-up led to the isolation of the complex $[(ZnBr)_2L^2] \cdot 4.5MeCN$ (**3**·4.5MeCN). The molecular structures of **1**, **2** and **3** are reported, together with their emission behaviour.

Keywords: Schiff-base; macrocycle; solvents; emission; DFT studies.

1. Introduction

Fluorescent organic materials are attracting current interest in areas such as optoelectronics and cellular imaging. [1-3] Organic materials usually give bright emission at a specific wavelength, although certain materials exhibit solvatochromism, which is the change in the optical properties of a material upon a change of the solvent polarity. A good example is *trans*-4-dimethylamino-4'-(1-oxybutyl)stilbene (DOS), which exhibits solvatochromism across the entire visible spectrum with shifts of hundreds of nanometers. [4] Whilst solvatochromic materials have potential applications in bio- and environmental sensing, such applications (molecular recognition and ion sensing) are well established in macrocyclic chemistry. [5] Combining solvatochromism with the inherent molecular recognition properties of macrocycles, opens up the possibility of intriguing bimodal sensing possibilities. Furthermore, Schiff-base compounds have attracted attention over the years primarily for their biological activity, [6-10] thus macrocyclic Schiff bases are of potential interest given their multiple binding sites. [11-12] We have been investigating the Robson-type Schiff-base macrocyclic family, derived from the [2+2] condensation of a diamine with a dialdehyde, specifically herein 1,3-diformylphenol in combination with the dianiline 2,2'-oxydianiline, 2-(2-aminophenoxy)aniline, $(2-NH_2C_6H_4)_2O$ (see chart 1). [13-17] We report the emission properties of the resulting macrocycles in various solvents, which reveals that the emission can be tuned by *ca.* 77

nm. Experimental observations are backed up by theoretical (DFT) calculations. Interestingly, a series of zinc complexes bearing phenol compartmental-type ligation were recently found to exhibit controllable photophysical properties by manipulation of the substituent (Me, *t*Bu, Cl) positioned *para* to the phenolic group. [18] With this in mind, we have also prepared herein zinc derivatives of L^1H_2 and L^2H_2 (see chart 2) and have investigated their emission behaviour.

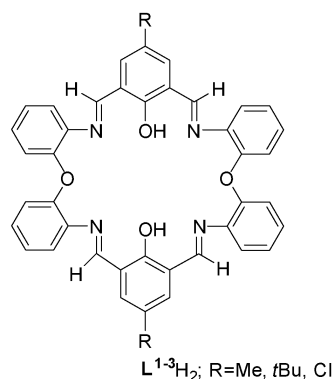


Chart 1. Schiff-base macrocycles $L^{1-3}H_2$

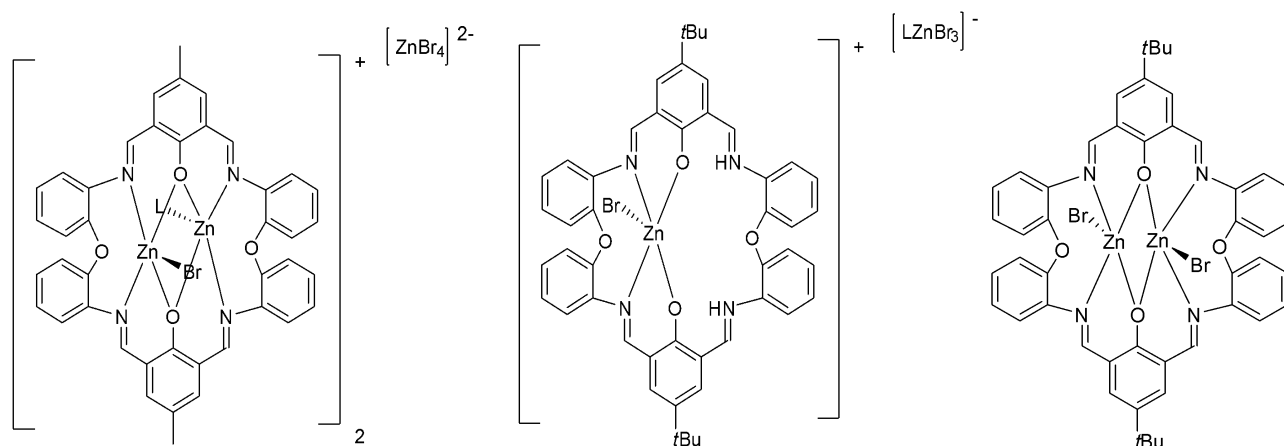


Chart 2. Complexes **1** to **3** (L = MeCN).

2. Materials and Methods

2.1 General

Solvents were dried using standard protocols, for example, toluene was refluxed over sodium/benzophenone, acetonitrile and dichloromethane were refluxed over calcium hydride, [19]

acetone was dried over magnesium sulfate, ethylacetate was dried over molecular sieves and dimethylsulfoxide was stored over barium oxide and distilled over calcium hydride prior to use.

The precursors 2,6-(CHO)₂-4-R-C₆H₂OH and (2-NH₂C₆H₄)₂O and the Schiff-base macrocycles were prepared by the literature methods. [20]

¹H NMR spectra were recorded on a Varian VXR 400 S spectrometer at 400 MHz at room temperature and were calibrated against the residual protio impurity of the deuterated solvent. UV-vis absorption spectra were recorded by JENWAY 7315 spectrophotometer. Photoluminescence emission spectra were collected in a quartz cuvette (10 × 10 mm), using a PerkinElmer LS55 spectrophotometer with an excitation slit width of 10 nm and an emission slit width set at 5 nm. The measurements were performed at standard pressure and room temperature. The sample was recorded on a Carl Zeiss Evo-60 SEM instrument and Imaging was performed with a LaB6 emitter. The absolute lifetime measurements were carried out with a FLS1000 photoluminescence spectrometer. The decay curves were analysed by deconvoluting the observed decays with the instrument response function (IRF) to obtain the intensity decay function, manifested as a sum of two exponentials for the present study. IR spectra were recorded on a Nicolet Avatar 360 FT-IR spectrometer. Elemental analyses were performed by the elemental analysis service at the University of Hull and Nanjing University of Information Science & Technology. Mass spectrometry was performed using a Bruker HCT-Ultra mass spectrometer.

2.2 Synthesis of **1**

To L¹H₂ (1.00 g, 1.52 mmol) and 3 equivalents of ZnBr₂ (1.03 g, 4.56 mmol) was added toluene (20 mL) and the system was refluxed for 12 h in the presence of 2 equivalents of Et₃N. On cooling, volatiles were removed *in vacuo*, and the residue was extracted into MeCN (20 mL). Standing at ambient temperature afforded yellow prisms of **1**. Yield 0.43 g, 24.5%. ¹H NMR (C₆D₆, 400 MHz): δ

8.18 (s, 2H, CH=N), 8.04 (s, 2H, CH=N), 7.84-6.34 (m, 20H, Ar-H), 1.80 (s, 6H, Me). IR (KBr, cm^{-1}): 2923 (s), 2853 (s), 2726 (w), 2349 (w), 2307 (w), 1623 (m), 1605 (m), 1590 (m), 1546 (m), 1462 (s), 1377 (s), 1304 (m), 1261 (m), 1235 (m), 1216 (m), 1150 (w), 1094 (m), 1071 (m), 1020 (m), 873 (w), 841 (w), 800 (s), 760 (w), 722 (s), 663 (w), 527 (w). M. S. Found (ESI): 899 [M-MeCN-Zn₃Br] 865 [M⁺-MeCN]. Elemental analysis calculated for C_{85.8}H₅₇Br_{6.10}N_{8.9}O₈Zn₅ (sample dried *in vacuo* for 12 h): C 46.90, H 2.61, N 5.67%. Found C 46.98, H 2.69, N 5.74%.

2.2 Synthesis of **2**

To L²H₂ (1.00 g, 1.36 mmol) and 2 equivalents of ZnBr₂ (0.69 g, 2.72 mmol) was added toluene (20 mL) and the system was refluxed for 12 h. On cooling, volatiles were removed *in vacuo*, and the residue was extracted into MeCN (20 mL). Standing at ambient temperature afforded orange prisms of **2**. Yield 1.08 g, 58.4 %. ¹H NMR (C₆D₆, 400 MHz): δ 7.70 (s, 2H, CH=N), 7.62 (s, 2H, CH=N), 7.30-6.06 (m, 20H, Ar-H), 1.94 (s, 1H, C=N-H), 1.71 (s, 1H, C=N-H), 1.02 (s, 18H, *t*Bu). IR (KBr, cm^{-1}): 3419(s) 2923 (s), 2854 (s), 2726 (s), 2671 (w), 2306 (w), 2279 (w), 2245 (w), 1637 (s), 1623 (s), 1593 (m), 1533 (m), 1463 (s), 1377 (s), 1336 (w), 1326 (w), 1309 (w), 1261 (m), 1237 (m), 1221 (m), 1180 (m), 1152 (m), 1097 (m), 1060 (m), 1021 (w), 980 (m), 934 (w), 942 (w), 904 (w), 875 (w), 849 (m), 805 (m), 773 (w), 754 (m), 740 (m), 723 (m), 695 (w), 622 (w), 569 (m), 554 (m), 524 (m), 507 (m), 478 (m), 453 (m), 445 (w). M. S. Found (ESI) 929 [M-ZnBr₃] 887 [M⁺]. Elemental analysis calculated for C₄₈H_{43.87}Br₄N₄O₄Zn_{2.07} (sample dried *in-vacuo* for 12 h): C 48.18, H 3.68, N 4.68%. Found C 48.28, H, 3.77, N 4.72%.

2.3 Synthesis of **3**

To L²H₂ (1.00 g, 1.36 mmol) and 2 equivalents of ZnBr₂ (0.69 g, 2.72 mmol) was added toluene (20 mL) and the system was refluxed for 12 h in the presence of 2 equivalents of Et₃N. On cooling, volatiles were removed *in vacuo*, and the residue was extracted into MeCN (20 mL). Standing at

ambient temperature afforded orange prisms of **3** Yield 0.96 g, 69.0 %. ^1H NMR (C_6D_6 , 400 MHz): δ 7.76 (s, 2H, CH=N), 7.62 (s, 2H, CH=N), 7.29-6.37 (m, 20H, Ar-H), 1.03. (s, 18H, *t*Bu). IR (KBr, cm^{-1}): 2923 (s), 2854 (s), 2727 (w), 1624 (m), 1606 (m), 1587 (m), 1463 (s), 1377 (s), 1322 (m), 1259 (s), 1222 (m), 1181 (m), 1099 (m), 1063 (s), 1021 (m), 979 (m), 843 (w), 800 (s), 754 (m), 738 (m), 701 (w), 630 (w), 571 (w), 525 (m), 474 (m). M. S. Found (ESI): 951 [M-Br], 804 [M-ZnBr₂], 765.4 [M-Zn₂Br₂]. Elemental analysis calculated for $\text{C}_{48}\text{H}_{42}\text{Br}_2\text{N}_4\text{O}_4\text{Zn}_2$ (sample dried *in vacuo* for 12 h): C 56.00, H 4.11, N 5.44%. Found C 56.08, H 4.19, N 5.58%.

2.4 Emission studies

Zn complexes (2 mg) were dissolved in 10 mL of the various named solvents (the concentration for the solutions for Zn complex **1**, **2** and **3** is 0.09 mmol/L, 0.19 mmol/L and 0.15 mmol/L, respectively), and then 1 ml was taken from the above solution, diluted to 5 mL and then used to record the UV-vis spectra. The fluorescence spectra test employed half the concentration of the solution, which was used for the UV-vis test. For complex **1**, the emission and excitation slit width employed was 15 nm and 7 nm, respectively. The emission and excitation slit width for complex **2** was 6 nm and 6 nm, respectively, whilst that for complex **3** was 7 nm and 3.5 nm, respectively.

2.5 X-ray Crystallography

Single crystal X-ray diffraction data were collected at the UK National Crystallography service using Rigaku Oxford Diffraction ultra-high intensity instruments employing modern areas detectors. In all cases standard procedures were employed for integration and processing of data.

Crystal structures were solved using dual space methods implemented within SHELXT. [21] Completion of structures was achieved by performing least squares refinement against all unique F^2 values using SHELXL-2018. [22] All non-H atoms were refined with anisotropic displacement parameters. Hydrogen atoms were placed using a riding model. Where the location of hydrogen atoms

was obvious from difference Fourier maps, CH and O-H bond lengths were refined subject to chemically sensible restraints. Minor disorder was treated using standard methods.

SQUEEZE [23] was used to model the disordered solvent in structure **1** and **3**.

3. Results and Discussion

3.1 Emission studies on $L^{1-3}H_2$

The [2+2] Schiff base macrocycles of type L^nH_2 are readily available in high yield *via* the reaction of 2,6-dicarboxy-4-R-phenol, where R = Me (n = 1), *t*Bu (n = 2) or Cl (n = 3), with 2,2'-oxydianiline, (2-NH₂C₆H₄)₂O. [18] These condensation products {[2-(OH)-5-(R)C₆H₂-1,3-(CH)₂][(O)(2-C₆H₄N)₂]}₂ (R = Me L^1H_2 , *t*Bu L^2H_2 , Cl L^3H_2) can be recrystallized from a variety of solvents.

The 'dried' macrocycle was strongly luminescent as a solid with an emission maximum at 585 nm. The Schiff base was also dissolved in a number of solvents, in order of decreasing dipole moment: acetonitrile (3.92), acetone (2.88), ethyl acetate (1.78), dichloromethane (1.60), and toluene (0.37).

The samples were excited at 400 nm, and the emission spectra for L^1H_2 , L^2H_2 and L^3H_2 are shown in Figure S1. In the case of L^3H_2 , the emission spectrum displays the full hypochromic shift of the macrocycle emission in different solvents, from λ_{max} at 508 nm (in acetonitrile) to 585 nm (in CH₂Cl₂); in most cases, components at both 508 and 585 nm are visible. For L^3H_2 , in acetonitrile the former (508) is far more pronounced, whilst for L^1H_2 , the 508 component is visible in acetonitrile, acetone and ethyl acetate; in all cases the 508 component is more pronounced in order of increasing dipole moment. The emission is typically broad, with full width at half maximum (FWHM) of 67±2 nm. Typically, the solutions with the largest dipole (acetonitrile) emit towards the blue/green end of the spectrum, whilst the macrocycle in the less polar solvents emits in the red end of the visible spectrum. Given this, we extended our studies to DMSO (dipole moment 3.96), for which the wavelengths exhibited peaks at a) 490 and 588 nm, b) 520 nm and c) 520 and 578 nm, for $L^{1-3}H_2$ respectively, results which were consistent with the observed dipole *versus* emission trend. It is thought that these the influence of the

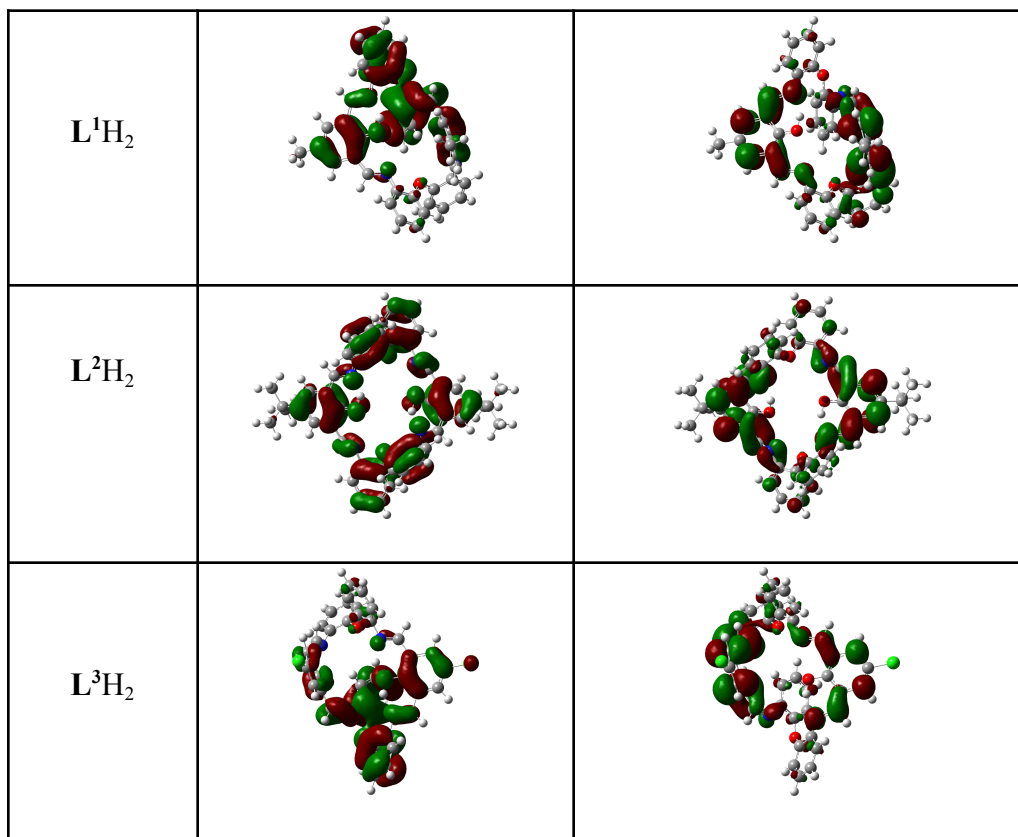
solvent on the intramolecular H-bonding is responsible for the observed hypochromic shifts. Given this, we recorded the ^1H NMR spectra of the most soluble macrocycle L^2H_2 in solvents of differing polarity in order to observe if there was any change to the value of δ_{OH} . Even the solubility of L^2H_2 was problematic, however we were able to record spectra in $\text{dms}\text{-d}_6$ (dipole moment 3.96), acetone-d_6 (dipole moment 2.88), THF-d_8 and C_6D_6 (dipole moment 0), for which δ_{OH} appeared at 14.86 ($\text{dms}\text{-d}_6$), 14.46 (acetone-d_6), 14.33 (THF-d_8) and 14.25 ppm (C_6D_6), respectively. There is in general a downfield shift of the δ_{OH} on increasing solvent polarity; such observations have been noted previously for intramolecular hydrogen bonding. [24]

3.2 DFT studies on L^{1-3}H_2

To provide explicit evidence for the energy states, in particular, the effect of the different solvents on the intramolecular H-bonding, the energy bandgaps of L^{1-3}H_2 were further evaluated by density function theory (DFT) calculations at the B3LYP/6-31G* level. As shown in Table 1, the three compounds L^{1-3}H_2 exhibited different shapes for the HOMO/LUMO orbitals in different molecular fragments, due to the different electronic ability of the donor and acceptor groups, namely methyl, *t*-Bu group and Cl. Using L^3H_2 as an example, the orbital distributions of the HOMO and LUMO energy levels were well separated on the parts of the naked phenyl ring and chloride-substituted phenyl ring, respectively. This push-pull system can contribute to adjust the energy gap in different solvents by intermolecular charge transfer (ICT).

Table 1. HOMOs and LOMOs for top L^1H_2 ; middle L^2H_2 ; bottom L^3H_2 .

| Compound | HOMO | LUMO |
|----------|------|------|
|----------|------|------|



Further, the effect of solvent polarity on the molecular conformation was also investigated by DFT calculations. It is noteworthy that the energy gap increases as the solvent polarity increased, and the relationship between the solvent polarity and energy gap (ΔE) is plotted in Figure 1. The intramolecular hydrogen bond (H-bond) was calculated from optimized molecular structure. For example, obviously, in compound L^3H_2 , the distance of H-bond in non-polarity n-hexane solvent (3.44 Å) is shorter than its in polarity solvent DMF (3.60 Å). We speculate that the intramolecular hydrogen bond in this system may play an important role to fix the molecular conformation, which can make the molecule more rigid and suppress the TICT and produce a hypochromic shift of the macrocycle emission in different solvent. This theoretic calculation was consistent with the experimental observations described above.

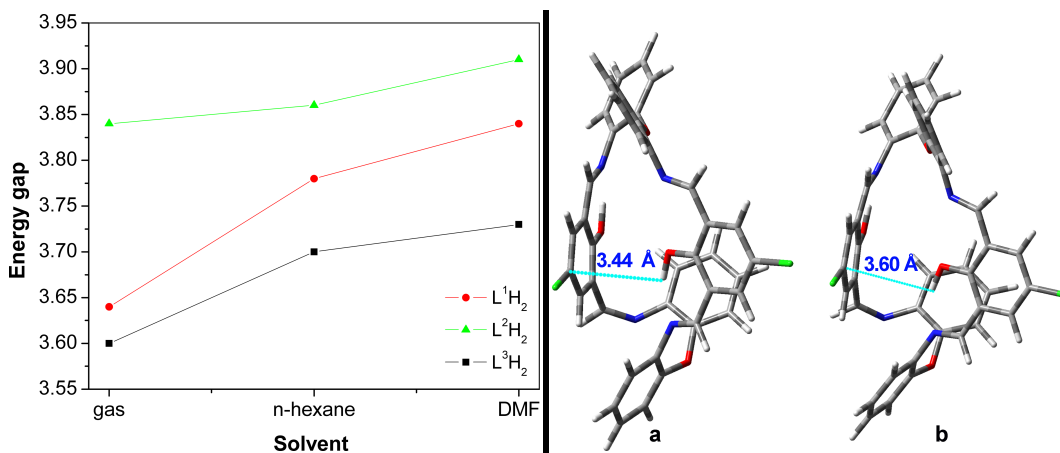


Figure 1. Theoretic calculation (B3LYP/6–31G* level) on the energy gap of compounds L¹⁻³H₂ in different solvents.

Table 2. HOMO/LUMO energy levels for L¹⁻³H₂

| Compound | HOMO | LUMO | Energy gap | Comments |
|-------------------------------|-------|-------|------------|---------------------|
| L ¹ H ₂ | -5.36 | -1.52 | 3.84 | In gas phase |
| | -5.74 | -1.88 | 3.86 | In <i>n</i> -hexane |
| | -6.01 | -2.10 | 3.91 | In DMF |
| L ² H ₂ | -5.33 | -1.69 | 3.64 | In gas phase |
| | -5.82 | -2.04 | 3.78 | In <i>n</i> -hexane |
| | -5.96 | -2.12 | 3.84 | In DMF |
| L ³ H ₂ | -5.61 | -2.01 | 3.60 | In gas phase |
| | -6.01 | -2.31 | 3.70 | In <i>n</i> -hexane |
| | -6.07 | -2.34 | 3.73 | In DMF |

3.3 Zinc complexes

We have investigated the coordination chemistry of the oxy-bridged macrocycles {[2-(OH)-5-(R)-C₆H₂-1,3-(CH₂)₂][O(2-C₆H₄N)₂]}₂ (R = Me, *t*Bu) with Zn²⁺. Reaction of L¹H with 3 equivalents of [ZnBr₂] afforded, following work-up, the complex [(ZnBr)(ZnNCMe)L¹]₂[ZnBr₄]·2.5MeCN (**1**·2.5MeCN) as orange crystals in moderate yield. Single crystals were grown from a saturated solution of acetonitrile at ambient temperature, and the molecular

structure is shown in Figure 2; selected bond lengths and angles are given in the Table 3. In the cation, the zinc centre (Zn1) is five-coordinated with a distorted trigonal bipyramid geometry ($\tau = 0.57$), and is bound by two phenoxide oxygens and the two nitrogens N1 and N2 of the macrocycle plus one bromide. However, Zn2 is five-coordinated by two phenoxide oxygens two nitrogens and an MeCN ligand, which overall creates a distorted trigonal bipyramid geometry at the metal ($\tau = 0.55$) [25].

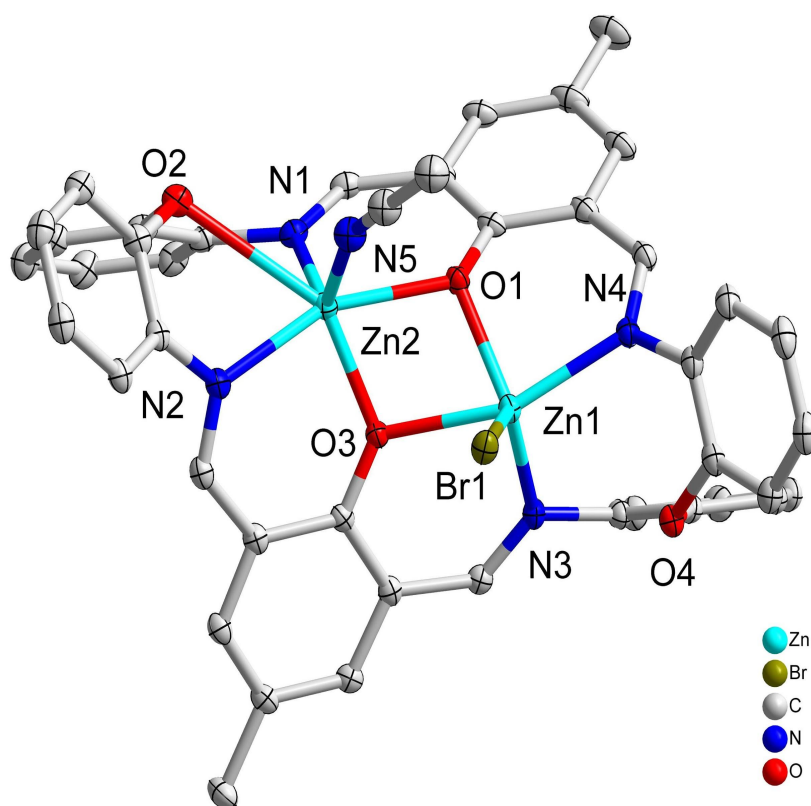


Figure 2. The molecular structure of **1**·2.5MeCN. Solvent and hydrogen atoms are omitted for clarity. Thermal ellipsoids are drawn at the 30% probability level.

In the case of L^2H_2 , reaction with 2 equivalents $ZnBr_2$ afforded, was found to be the salt following work-up the complex $[(ZnBr)L^2H_2][ZnBr_3NCMe] \cdot 3MeCN$ (**2**·3MeCN) in *ca.* 58.4% isolated yield as shown in Figure 3. Zn centre in complex **2** is five-coordinated and adopt distorted trigonal bipyramid

geometrie with a τ value of 0.67. Notably, on attempting to add Et_3N in the reaction between L^2H_2 and ZnBr_2 , the orange crystalline complex $[(\text{ZnBr})_2\text{L}^2]\cdot 4.5\text{MeCN}$ (**3** $\cdot 4.5\text{MeCN}$) which is shown in Figure 4 was successfully synthesized and isolated in *ca.* 69.0 % isolated yield. The zinc centres adopt distorted trigonal bipyramid geometries with a bromide at each apex ($\tau=0.76$). The bridging phenoxide oxygens O1 and O2 and the nitrogens N1 and N4 form the basal plane. Selected bond lengths in these structures are shown in **Table 3**. In these solvates, the range of C=N bond lengths [1.287(9)–1.300(4) Å] compares favourably with those reported for the related oxygen bridged phenolic macrocycles [1.276(2)–1.381(4) Å] [20].

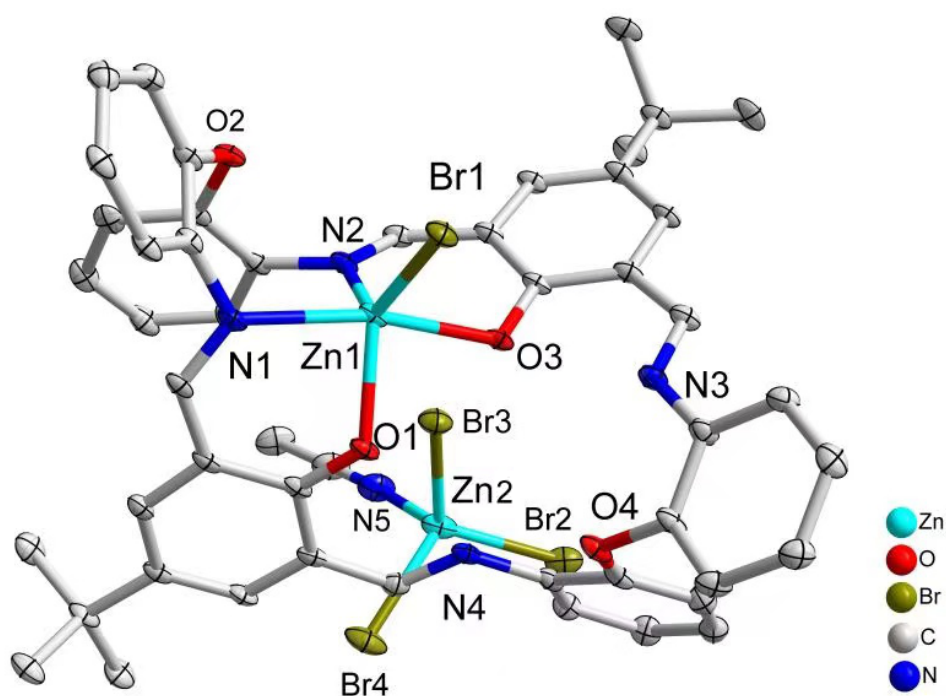


Figure 3. The molecular structure of **2** $\cdot 3\text{MeCN}$. Solvent and hydrogen atoms are omitted for clarity. Thermal ellipsoids are drawn at the 30% probability level.

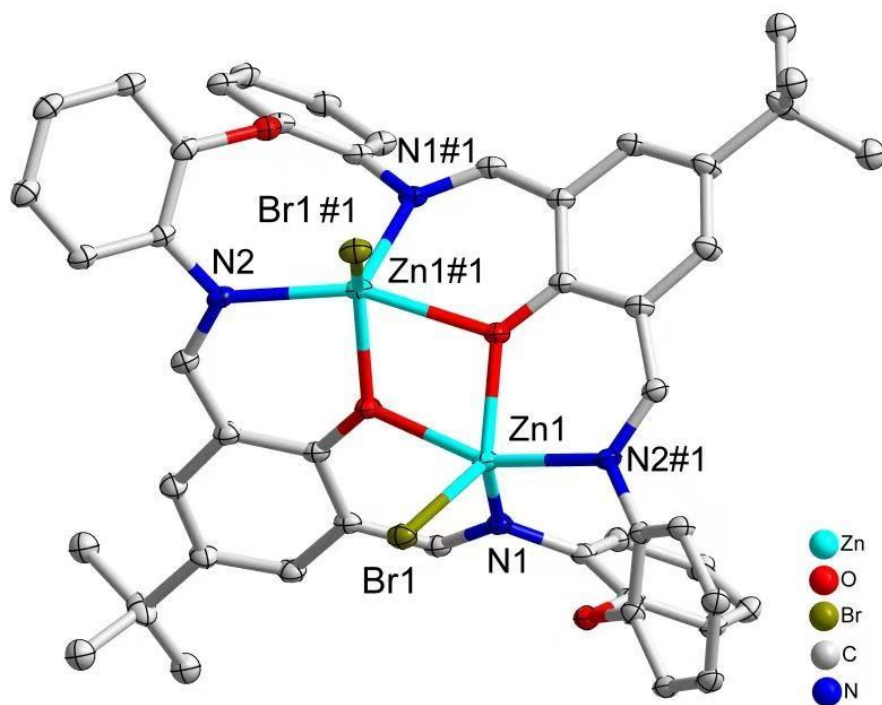


Figure 4. The molecular structure of **3**·4.5MeCN. Solvent and hydrogen atoms are omitted for clarity.

Thermal ellipsoids are drawn at the 30% probability level. (Symmetry Operators #a: 1-x, y, 1.5-z)

In the infrared spectra of the Zn(II) complexes, strong stretching bands for =CH-NH- fragment were absent, but strong, sharp bands in the range of 1623–1625 cm^{-1} can be assigned to the azomethine C=N stretching frequency[26]. In contrast to the spectra observed for **1** and **3**, that for **2** contained an absorption band at 3419 cm^{-1} consistent with the presence of protonated amine (NH^+) in the structure.

Table 3. Selected bond lengths (\AA) and angles ($^\circ$) in **1**, **2** and **3**.

119.55(10)

| | Selected bonds | Length (\AA) | Selected angles | ($^\circ$) |
|------------------|----------------|-------------------------|------------------|--------------|
| Complex 1 | Zn(1)-O(1) | 2.054(2) | O(1)-Zn(1)-N(4) | 84.15(10), |
| | Zn(1)-N(3) | 2.098(3) | N(3)-Zn(1)-O(3) | 82.90(10), |
| | Zn(1)-O(3) | 2.121(2) | N(3)-Zn(1)-N(4) | 103.42(11), |
| | Zn(1)-Br(1) | 2.400(5) | N(4)-Zn(1)-O(3) | 156.32(10) |
| | Zn(2)-O(3) | 2.023(2) | O(1)-Zn(2)-Br(2) | 92.30(2) |
| | Zn(2)-N(1) | 2.045(3) | O(1)-Zn(2)-N(2) | 156.31(10) |
| | Zn(2)-N(5) | 2.073(4) | O(3)-Zn(2)-N(1) | 110.63(10), |
| | Zn(2)-O(1) | 2.104(2) | N(1)-Zn(2)-Br(2) | 113.2(2) |
| | Zn(2)-Br(2) | 2.571(10) | N(5)-Zn(2)-N(2) | 94.63(13) |

| | | | | |
|------------------|-------------|------------|------------------|-----------|
| Complex 2 | N(1)-Zn(1) | 2.171(5) | C(11)-N(1)-Zn(1) | 122.1(4) |
| | N(2)-Zn(1) | 2.106(5) | C(12)-N(1)-Zn(1) | 121.4(3) |
| | N(5)-Zn(2) | 2.088(7) | C(24)-N(2)-C(23) | 118.2(5) |
| | O(1)-Zn(1) | 2.001(4) | C(24)-N(2)-Zn(1) | 126.2(4) |
| | O(3)-Zn(1) | 2.136(4) | C(23)-N(2)-Zn(1) | 115.6(4) |
| | Zn(1)-Br(1) | 2.3799(9) | | |
| Complex 3 | Zn(1)-O(1) | 2.018(5) | O(1)-Zn(1)-N(3) | 110.7(2) |
| | Zn(1)-N(3) | 2.042(5) | O(1)-Zn(1)-O(3) | 74.06(17) |
| | Zn(1)-O(3) | 2.103(5) | N(3)-Zn(1)-O(3) | 86.9(2) |
| | Zn(1)-N(2) | 2.121(5) | O(3)-Zn(1)-N(2) | 156.1(2) |
| | Zn(2)-O(3) | 2.052(5) | O(1)-Zn(1)-N(5) | 125.4(2) |
| | Zn(2)-N(1) | 2.099(6) | O(3)-Zn(1)-N(4) | 84.1(2) |
| | Zn(2)- N(4) | 2.105(6) | N(1)-Zn(2)-N(4) | 103.6(2) |
| | Zn(2)- O(1) | 2.123(4) | | |
| | Zn(2)-Br(1) | 2.4011(11) | | |

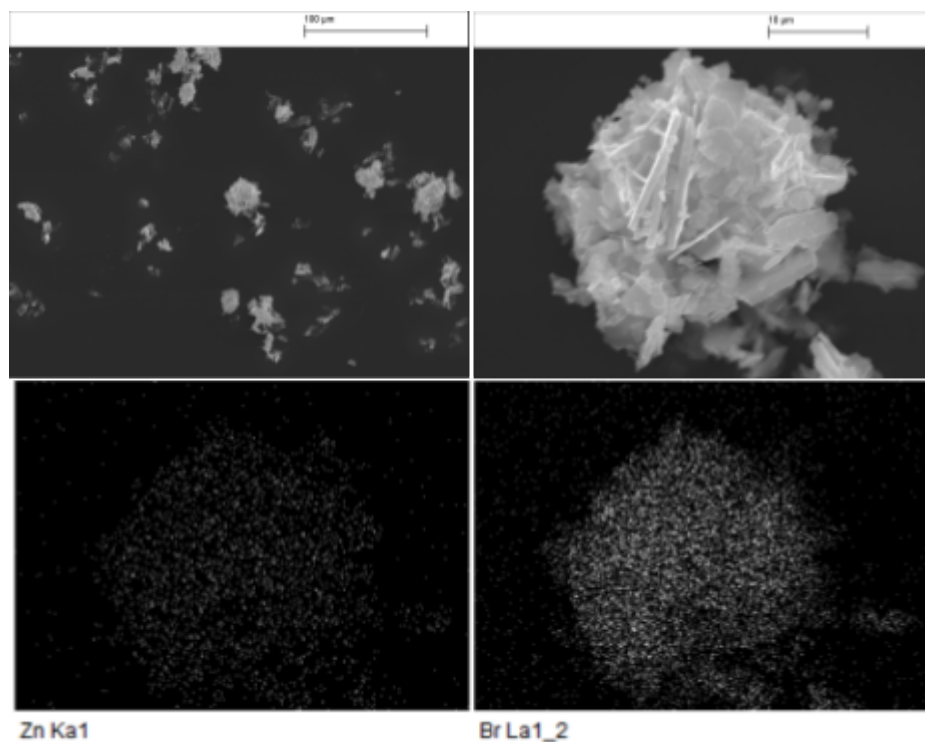


Figure 5. SEM and mapping images of complex 2.

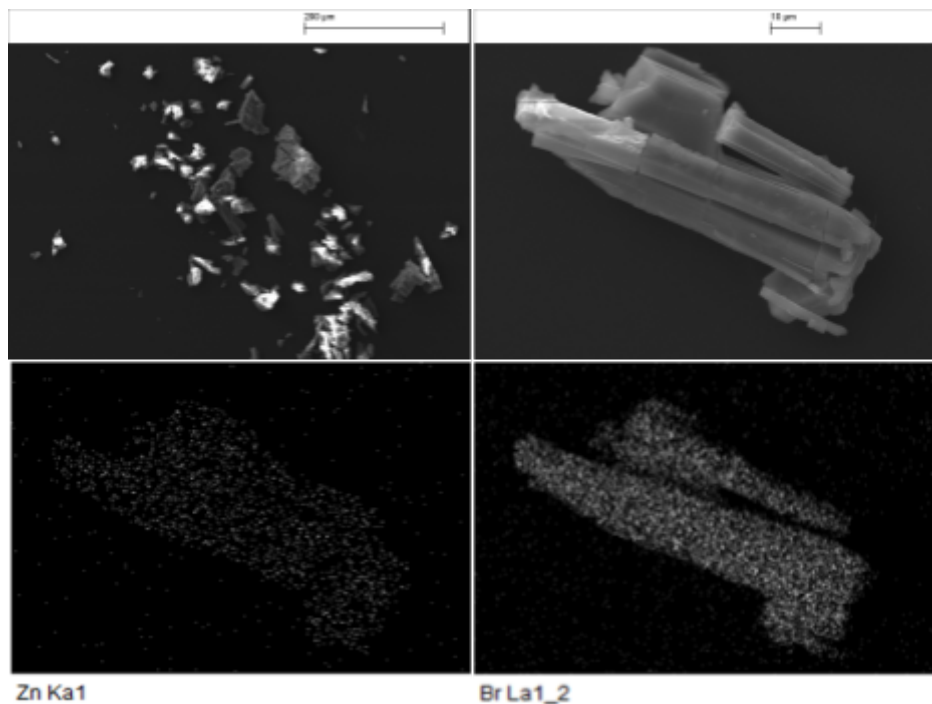


Figure 6. SEM and mapping images of complex **3**.

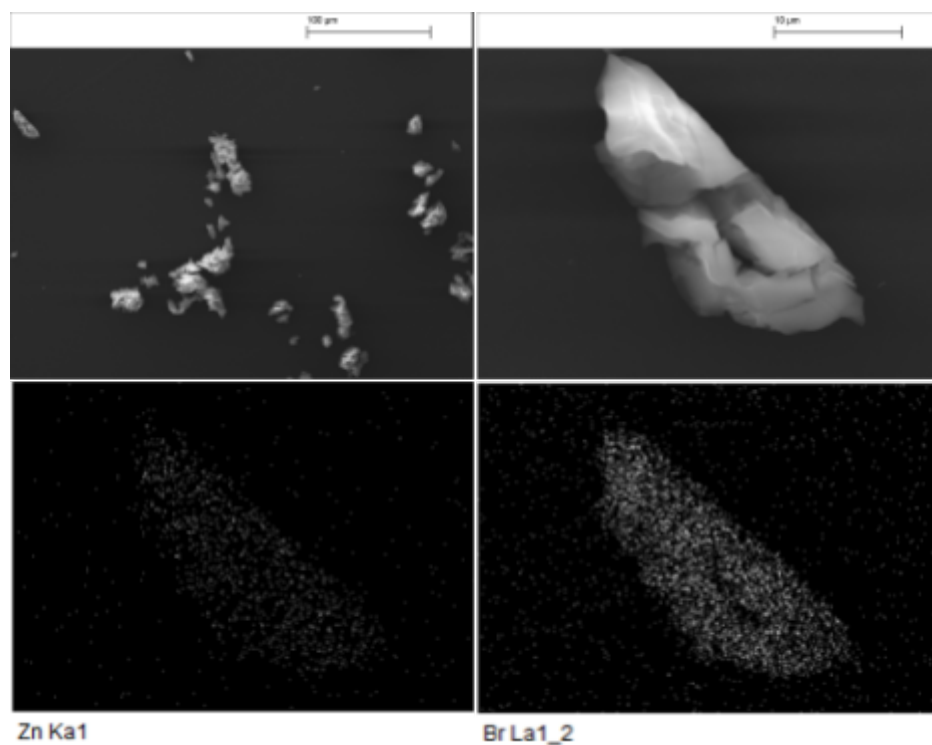


Figure 7. SEM and mapping images of complex **3**.

The surface morphology of Zn(II) complexes was analyzed by scanning electron microscopy (SEM) as depicted in Figs. 5-7. Figure 5 shows a SEM micrograph of complex **1**, where stacked plate shape

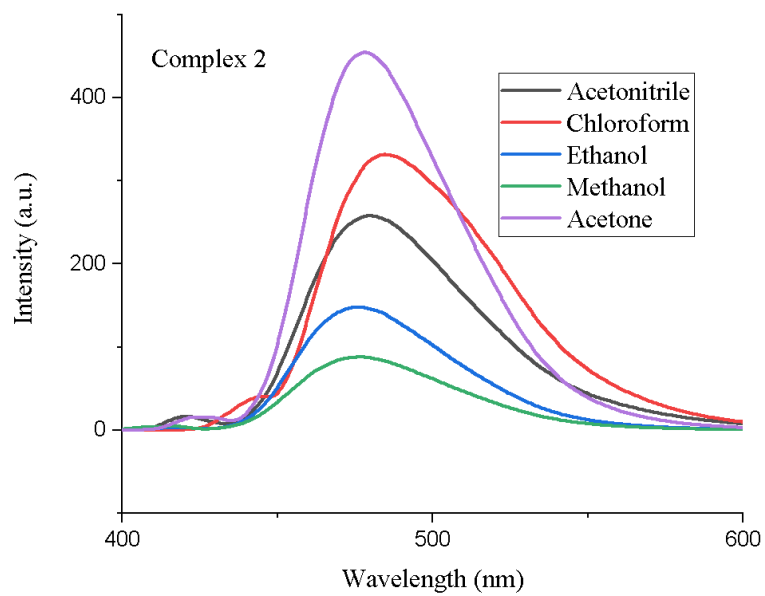
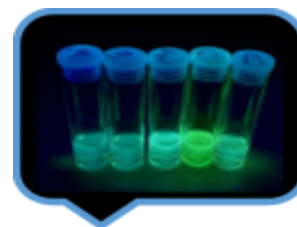
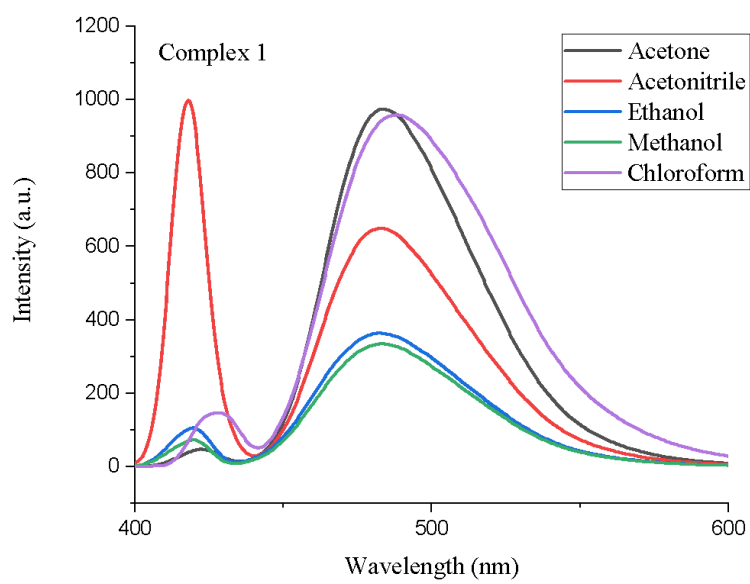
crystals are observed with the particle size range from 5 to 15 μm . Figure 6 depicts the nano rod-like structure of complex **2** with the diameter ranging from 10 to 50 μm . The SEM image of complex **3**, as shown in Figure 7, revealed accumulated lumpy-like crystals.

3.4 Emission studies on the Zn Complexes

The UV-vis absorption spectra of the Zn complexes in different solvents (methanol, ethanol, chloroform, acetonitrile, acetone) were recorded at room temperature, and the data are interpreted in Table 4 and Figure S2. The first band centered at 280–330 nm can be assigned to a π - π^* transition of the phenyl rings. The second absorption band in the range 405–421 nm can be attributed to intramolecular interactions between metal and ligand [27].

The photoluminescence of the zinc complexes was examined as solid samples of **1–3** as well as in solutions different solvents (methanol, ethanol, acetonitrile, acetone, chloroform). Selected data are summarized in Table 4. Complex **1** exhibited an emission maximum at 478–482 nm and green-yellow luminescence in solution except for in methanol. The maxima emission peaks are bathochromically shifted by around 50 nm in methanol compared with those in other solvents, due to the high polarity of the solvent. Similar to complex **1**, the maximum emission wavelengths of complex **2** were around 477–480 nm. Moreover, As shown in Figure 8, complex **3** with luminescent bands centred at 477 nm to 480 nm with green-yellow luminescence.

Luminescence properties of **1–3** were also examined in the solid state at 298 K (Figure 9). Complexes **1** and **3** exhibited similar luminescent bands centred at 509 and 520 nm, respectively. Notably, solid **2** exhibits a yellow emission (Figure S4) with λ_{max} at 564 nm. On comparing the solid-state spectra with the solution spectra, the maximum emission bands of the solid state of **1–3** are obviously red-shifted by 24–87 nm. These significant bathochromic shifts are caused by the difference in parameters like planarity, the irregular arrangement in the crystalline state and intermolecular forces such as π - π^* stacking and excimers of each molecule [28, 29].



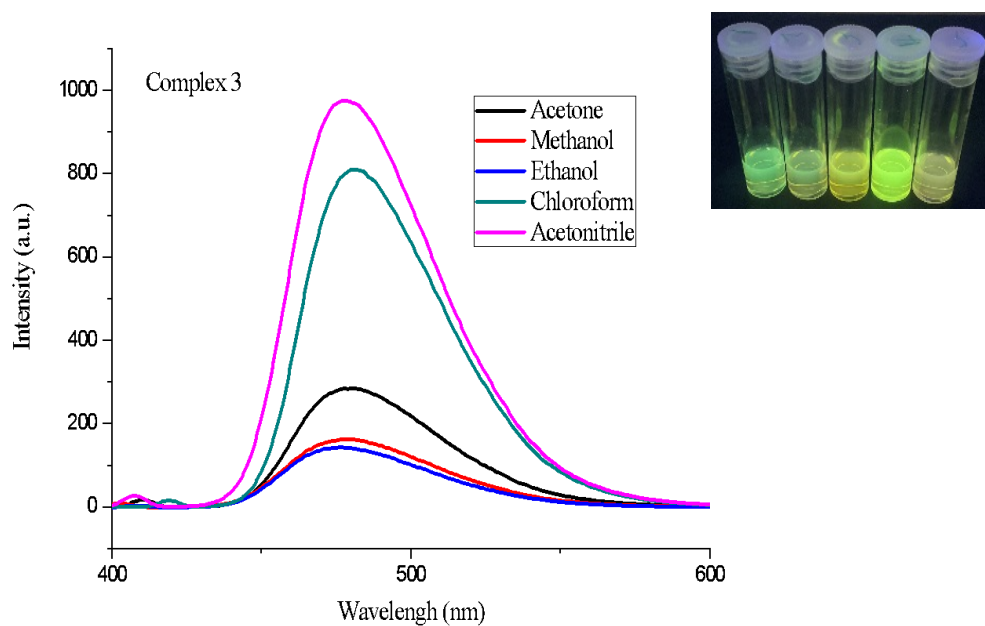


Figure 8. Photoluminescence emission spectra of complexes **1-3** in different solvents at 292 K and Fluorescent picture for Zn Complexes (Insert picture: Emission pictures for zinc complexes in different solvents; From left to right is Methanol; Ethanol; Acetonitrile; Chloroform; Acetone).

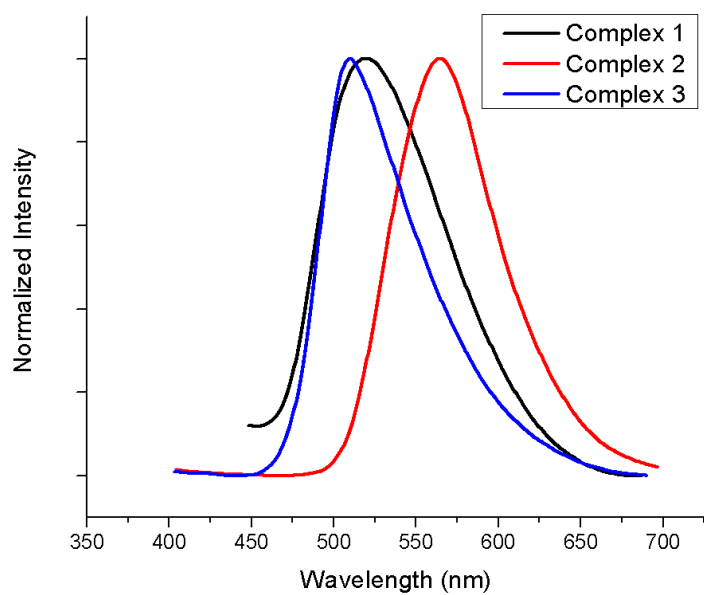


Figure 9. Solid Photoluminescence emission spectra of the Zn complexes.

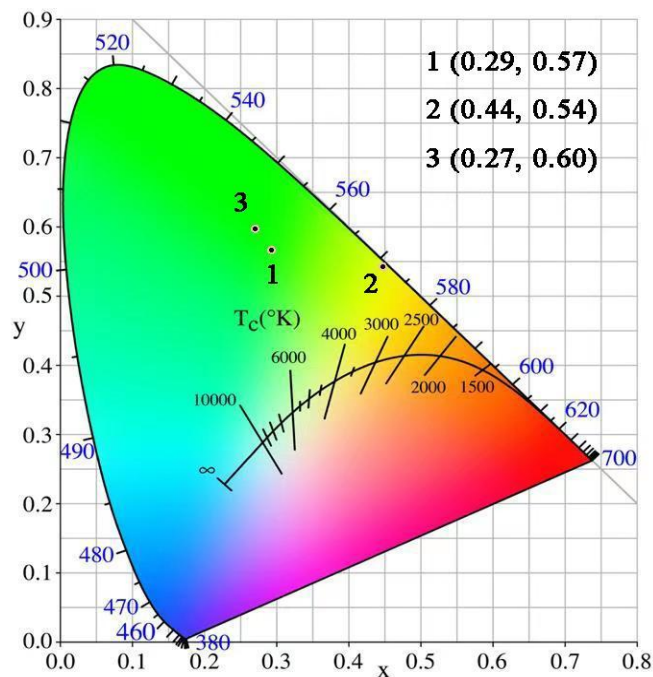


Figure 10. CIE diagram of Zn complexes in solid state Chromaticity parameters according to CIE 1931 colour.

The Commission Internationale de L'Eclairage (CIE) coordinates from Zn complexes solid photoluminescence spectra are shown in Figure 10. It worth noting that the emission wavelength of complexes **1** and **3** are approximately the same and they exhibit yellow fluorescence, but for complex **2** the maximum emission wavelength is 50 nm higher and it exhibits a yellow-green colour.

Luminescence quantum yields were measured for both solid samples and solutions by absolute measurement. As shown in Table 4, complexes **1-3** were found to exhibit moderate fluorescence quantum yields [30] in solution. In the solid state, the quantum yields for complex **1-3** is 2.66%, 6.90% and 1.29%, respectively, together with the high PL lifetime makes complex **2** good candidates as luminescent materials. The phenomenon in which complexes show higher photoluminescence efficiency in the aggregated state than in solution is related to aggregation-induced emission enhancement (AIEE) [31].

The lifetimes for the as-prepared Zn complexes **1-3** as solid-state samples were also recorded. The luminescence decay spectra and their fitted curves are shown in Figure S3. These decay curves have been fitted with the standard biexponential decay equation and were found to agree well. The observed lifetimes are 0.64, 29.8 and 0.36 ns for Zn complex **1**, **2** and **3**, respectively. The measured lifetime of **2** is significantly longer than the other two, which we attribute to a fast charge transfer process between the Zn(II) and the specific coordinated macrocycle. The lifetime on the nanosecond scale indicates that the Zn complexes have the fluorescent character of the luminescence [28].

Table 4. Emission data for zinc complexes.

| | λ_{abs} | $\lambda_{\text{em}} (\lambda_{\text{ex}})$ | Quantum yield (ϕ) ^a | fluorescence lifetime τ |
|----------------------------|------------------------|---|---------------------------------------|------------------------------|
| Zn1 in Methanol | 284, 409 | 484 (409) | <0.01 | 0.64 ns |
| Zn1 in Ethanol | 285, 410 | 482 (410) | 0.76 | |
| Zn1 in Acetonitrile | 285, 413 | 483 (413) | 2.34 | |
| Zn1 in Chloroform | 286, 419 | 488 (419) | 2.50 | |
| Zn1 in Acetone | 330, 413 | 484 (413) | 2.13 | |

| | λ_{abs} | $\lambda_{\text{em}} (\lambda_{\text{ex}})$ | Quantum yield (ϕ) ^a | fluorescence lifetime τ |
|----------------------------|------------------------|---|---------------------------------------|------------------------------|
| Zn2 in Methanol | 280, 405 | 479 (405) | <0.01 | 29.8 ns |
| Zn2 in Ethanol | 284, 406 | 482 (406) | 0.80 | |
| Zn2 in Acetonitrile | 290, 414 | 485 (414) | 0.24 | |
| Zn2 in Chloroform | 284, 430 | 484 (430) | 3.54 | |
| Zn2 in Acetone | 330, 416 | 478 (416) | 2.75 | |

| | λ_{abs} | λ_{em} | Quantum yield (ϕ) ^a | fluorescence lifetime τ |
|----------------------------|------------------------|-----------------------|---------------------------------------|------------------------------|
| Zn3 in Methanol | 282, 406 | 479 (406) | 0.38 | 0.36 ns |
| Zn3 in Ethanol | 286, 411 | 477 (411) | 1.07 | |
| Zn3 in Acetonitrile | 284, 410 | 478 (410) | 2.41 | |
| Zn3 in Chloroform | 286, 421 | 480 (421) | 3.13 | |
| Zn3 in Acetone | 330, 413 | 480 (413) | 2.96 | |

^a Absolute luminescence quantum yield measured by integrating sphere.

DFT studies for complex 3

Density function theory (DFT) calculations at the B3LYP/6–31G* level are provided for the energy states discussion. As shown in Table 4, the Zn complex **3** exhibited different shapes for the HOMO/LUMO orbitals. Using L³H₂ as an example, the orbital distributions of the HOMO energy

levels mainly separated on bromides but the LUMO energy levels were well separated on the whole macrocycle ligand.

Conclusion

In conclusion, the Schiff base macrocycles $L^{1-3}H_2$ exhibit hypochromic shifts of the emission bands. The features of the emission can be aligned with the dipole of the solvent system employed and is thought to be related to the influence of the solvent on the intramolecular hydrogen bonding. In the case of the zinc complexes, it was found that the Zn(II) complexes demonstrate yellow or yellow/green photoluminescence and enhanced performance *versus* the parent macrocycles. All the complexes exhibit good PL emissions and quantum yields in solutions. The lifetime measurement and solid-state quantum yields shows that complex **2** generates a longer-live fluorescence and relatively high quantum yields than the other two complexes. The potential application of such complexes in organic light emitting diodes and other luminescence-based devices is under investigation.

Acknowledgements

We thank the China Scholarship Council (CSC) for a PhD Scholarship to KW. We thank the EPSRC National Crystallographic Service at Southampton for data collection and the Physical Sciences Data Service Centre for access to the CCDC. CR thanks the EPSRC for a travel grant (EP/L012804/1). TB is grateful to an Alan Katritzky Scholarship awarded by UEA.

CCDC 2050837-2050839 contain the supplementary crystallographic data for complexes **1-3**. These data can be obtained free of charge via <http://www.ccdc.cam.ac.uk/conts/retrieving.html> or from the Cambridge Crystallographic Data Centre, 12 Union Road, Cambridge, CB2 1EZ, UK; fax (+44) 1223-336-033; or e-mail: deposit@ccdc.cam.ac.uk.

CONFLICT OF INTEREST

The authors declare no potential conflict of interest.

References

- [1] Askim J R, Mahmoudi M, Suslick K S. Optical sensor arrays for chemical sensing: the optoelectronic nose. *Chem. Soc. Rev.* 2013; 42(22): 8649-8682. <https://doi.org/10.1039/C3CS60179J>
- [2] Guo Z, Park S, Yoon J, Injae S. Recent progress in the development of near-infrared fluorescent probes for bioimaging applications. *Chem. Soc. Rev.* 2014; 43(1): 16-29. <https://doi.org/10.1039/C3CS60271K>
- [3] Zhang H, Sun T, Ruan Q, Zhao J L, Mu L, Zeng X, Jin Z W, Su S B, Luo Q Y, Yan Y Y, Redshaw C. A multifunctional tripodal fluorescent probe for the recognition of Cr^{3+} , Al^{3+} , Zn^{2+} , and F^- with controllable ESIPT processes. *Dyes and Pigments*, 2019, 162: 257-265. <https://doi.org/10.1016/j.dyepig.2018.10.025>
- [4] Reichardt C, Welton T. Solvents and solvent effects in organic chemistry, 4th Ed. Weinheim, Germany, Wiley-VCH, 2010.
- [5] Mullen K M, Beer P D. Sulfate anion templation of macrocycles, capsules, interpenetrated and interlocked structures. *Chem. Soc. Rev.* 2009; 38(6): 1701-1713. <https://doi.org/10.1039/B806041J>
- [6] Hodnett E M, Dunn W J. Structure-antitumor activity correlation of some Schiff bases. *J. Med. Chem.* 1970; 13(4): 768-770. <https://pubs.acs.org/doi/pdf/10.1021/jm00298a054>
- [7] Pandeya S N, Sriram D, Nath G, Clercq E D. Synthesis and antimicrobial activity of Schiff and Mannich bases of isatin and its derivatives with pyrimidine. *Il Farmaco* 1999, 54(9): 624-628. [https://doi.org/10.1016/S0014-827X\(99\)00075-0](https://doi.org/10.1016/S0014-827X(99)00075-0)
- [8] El-masry A H, Fahmy H H, Ali Abdelwahed S H. Synthesis and antimicrobial activity of some new benzimidazole derivatives. *Molecules* 2000; 5(12): 1429-1438. <https://doi.org/10.3390/51201429>
- [9] Jarrahpour A A, Zarei M. Synthesis of novel azo Schiff base bis [5-(4-methoxyphenylazo)-2-hydroxy-3-methoxy benzaldehyde]-1, 2-phenylene diimine. *Molbank* 2004; 2004(1): M377. <https://doi.org/10.3390/M377>

- [10] Siddiqui H L, Iqbal A, Ahmad S, Weaver G W. Synthesis and spectroscopic studies of new Schiff bases. *Molecules* 2006; 11(2): 206-211. <https://doi.org/10.3390/11020206>
- [11] Brooker S. Complexes of thiophenolate-containing Schiff-base macrocycles and their amine analogues. *Coord. Chem. Rev.* 2001; 222: 33. [https://doi.org/10.1016/S0010-8545\(01\)00300-9](https://doi.org/10.1016/S0010-8545(01)00300-9)
- [12] Radecka-Paryzek W, Patroniak V, Lisowski J. Metal complexes of polyaza and polyoxaaza Schiff base macrocycles. *Coord. Chem. Rev.* 2005; 249(21-22): 2156-2175. <https://doi.org/10.1016/j.ccr.2005.02.021>
- [13] Arbaoui A, Redshaw C, Hughes D L. Multinuclear alkylaluminium macrocyclic Schiff base complexes: influence of procatalyst structure on the ring opening polymerisation of ϵ -caprolactone. *Chem. Commun.* 2008; (39): 4717-4719. <https://doi.org/10.1039/B810417D>
- [14] Arbaoui A, Redshaw C, Hughes D L. One-pot conversion of tetraiminodiphenols to diiminodiaminodiphenols via methyl transfer at aluminium. *Supramol. Chem.* 2009; 21(1-2): 35-43. <https://doi.org/10.1080/10610270802438846>
- [15] Yang W., Zhao K Q, Wang B Q, Redshaw C, Elsegood M R, Zhao J L, Yamato T Manganese coordination chemistry of bis (imino) phenoxide derived [2+2] Schiff-base macrocyclic ligands. *Dalton Trans.* 2016; 45(1): 226-236. <https://doi.org/10.1039/C5DT03453A>
- [16] Chen H, Huang C, Deng Y, Sun, Q, Zhang, Q L, Zhu B X, Ni X L. Solvent-switched Schiff-base macrocycles: self-sorting and self-assembly-dependent unconventional organic particles. *ACS nano.* 2019, 13(3): 2840-2848. <https://doi.org/10.1021/acsnano.8b09478>
- [17] Chen H, Huang C, Ding Y, Zhang Q L, Zhu B X, Ni X L. Organic core-shell-shaped micro/nanoparticles from twisted macrocycles in Schiff base reaction. *Chem. Sci.*, 2019, 10(2), 490-496. <https://doi.org/10.1039/C8SC03824D>

- [18] Chakraborty P, Adhikary J, Samanta S, Majumder I, Massera C, Escudero D, Sanjib G, Antonio B, Antonio F, Das D. Influence of para substituents in controlling photophysical behavior and different non-covalent weak interactions in zinc complexes of a phenol based “end-off” compartmental ligand. *Dalton Trans.* 2015; 44(46): 20032-20044. <https://doi.org/10.1039/C5DT02768C>
- [19] Williams D B G, Lawton M. Drying of organic solvents: quantitative evaluation of the efficiency of several desiccants. *J. Org. Chem.* 2010; 75(24): 8351-8354. <https://doi.org/10.1021/jo101589h>
- [20] Yang W, Zhao K Q, Prior T J, Hughes D L, Arbaoui A, Elsegood M R J, Redshaw C. Structural studies of Schiff-base [2+2] macrocycles derived from 2, 2'-oxydianiline and the ROP capability of their organoaluminium complexes. *Dalton Trans.*, 2016, 45(30): 11990-12005. <https://doi.org/10.1039/C6DT01997H>
- [21] Sheldrick G. M. Crystal structure of 4-benzyl-2H-benzo[b][1,4]thiazin-3(4H)-one. *Acta Cryst.*, (2015). **A71**, 3-8. <https://doi.org/10.1107/S2056989015022276>
- [22] Sheldrick G. M. SHELXT - Integrated space-group and crystal-structure determination. *Acta Cryst.* (2015). **C71**, 3-8. <https://doi.org/10.1107/S2053273314026370>
- [23] A.L. Spek. PLATON SQUEEZE: a tool for the calculation of the disordered solvent contribution to the calculated structure factors. *Acta Cryst.* (2015). **C71**, 9-18. <https://doi.org/10.1107/S2053229614024929>
- [24] Dziembowska T, Malarski Z, Szczodrowska B. Solvent effect on the intramolecular hydrogen bond in 8-quinolinol N-oxide[J]. *J. Soln Chem.* 1996; 25(2): 179-189.
- [25] Addison A W, Rao T N, Reedijk J, van Rijn J, Verschoor G C. Synthesis, structure, and spectroscopic properties of copper (II) compounds containing nitrogen–sulphur donor ligands; the crystal and molecular structure of aqua [1, 7-bis (N-methylbenzimidazol-2'-yl)-2, 6-dithiaheptane] copper (II) perchlorate. *J. Am. Chem. Soc., Dalton Trans.*, 1984, 7: 1349-1356. <https://doi.org/10.1039/DT9840001349>

- [26] Marchetti F, Pettinari C, Di Nicola C, Tombesia A, Pettinari R. Coordination chemistry of pyrazolone-based ligands and applications of their metal complexes. *Coord. Chem. Rev.* 2019; 401: 213069. <https://doi.org/10.1016/j.ccr.2019.213069>
- [27] Gusev A, Shul'gin V, Braga E, Zamnius E, Kryukova M, Linert W. Luminescent properties of Zn complexes based on tetradentate N₂O₂-donor pyrazolone schiff bases. *Dyes and Pigments* 2020; 183: 108626. <https://doi.org/10.1016/j.dyepig.2020.108626>
- [28] Lakshmanan R, Shivaprakash N C, Sindhu S. Switching from sky blue to deep green fluorescent Zn (II) complexes for OLEDs applications. *J. Lumin.* 2018; 196: 136-145. <https://doi.org/10.1016/j.jlumin.2017.12.031>
- [29] Yang M, Xu D, Xi W, Wang L, Zheng J, Huang J, Zhang J, Zhou H, Wu J, Tian Y. Aggregation-induced fluorescence behavior of triphenylamine-based Schiff bases: the combined effect of multiple forces. *J. Org. Chem.* 2013; 78: 10344–10359. <https://doi.org/10.1021/jo401719c>
- [30] Xia J, Zhou Z, Li W, Zhang H Q, Redshaw C, Sun W H. Synthesis, structure and fluorescent properties of 2-(1H-benzoimidazol-2-yl) quinolin-8-ol ligands and their zinc complexes. *Inorg. Chim. Acta* 2013; 394: 569-575. <https://doi.org/10.1016/j.ica.2012.09.012>
- [31] Ren Y, Kan W H, Henderson M A, Bomben P G, Berlinguette C P, Thangadurai V, Baumgartne T. External-stimuli responsive photophysics and liquid crystal properties of self-assembled “phosphole-lipids”. *J. Am. Chem. Soc.* 2011; 133(42): 17014-17026. <https://doi.org/10.1021/ja206784f>.

Table 5. Crystallographic data for complexes **1 - 3**.

| Compound | 1 | 2 | 3 |
|----------|---|---|---|
|----------|---|---|---|

| Formula | $C_{87.80}H_{60}Br_{6.10}N_{9.90}O_8Zn_5 + 2.5MeCN$ | $C_{50}H_{46.87}Br_4N_5O_4Zn_{2.07} + 3MeCN$ | $C_{48}H_{42}Br_2N_4O_4Zn_2 + 4.5MeCN$ |
|---|---|--|--|
| Formula weight | 2298.45 | 1359.66 | 1029.41 |
| Crystal system | Monoclinic | Orthorhombic | Monoclinic |
| Space group | $C2/c$ | $P2_12_12_1$ | $P2/c$ |
| a (Å) | 32.5115(3) | 12.02380(10) | 13.4090(2) |
| b (Å) | 14.0969(10) | 13.95690(10) | 9.11430(10) |
| c (Å) | 20.3515(2) | 34.0092(2) | 23.1757(3) |
| α (°) | 90 | 90 | 90 |
| β (°) | 103.68(10) | 90 | 103.43(10) |
| γ (°) | 90 | 90 | 90 |
| V (Å ³) | 9092.7(14) | 5707.25(7) | 2754.92(6) |
| Z | 4 | 4 | 2 |
| Temperature (K) | 100(2) | 100(2) | 100(2) |
| Wavelength (Å) | 1.54178 | 1.54178 | 1.54178 |
| Calculated density (g.cm ⁻³) | 1.609 | 1.582 | 1.241 |
| Absorption coefficient (mm ⁻¹) | 5.098 | 4.757 | 3.080 |
| Transmission factors (min./max.) | 0.8116, 1.000 | 0.3681, 1.000 | 0.7059, 1.000 |
| Crystal size (mm ³) | 0.060 × 0.050 × 0.005 | 0.050 × 0.020 × 0.020 | 0.200 × 0.180 × 0.040 |
| θ (max) (°) | 70.40 | 70.02 | 68.23 |
| Reflections measured | 50225 | 132576 | 48389 |
| Unique reflections | 8556 | 10763 | 5023 |
| R_{int} | 0.0295 | 0.0563 | 0.0296 |
| F(000) | 4334 | 2727 | 1040 |
| Number of parameters | 538 | 676 | 284 |
| $R_1 [F^2 > 2\sigma(F^2)]$ | 0.0457 | 0.0420 | 0.0416 |
| wR_2 (all data) | 0.1227 | 0.1074 | 0.1040 |
| GOOF, S | 1.031 | 1.077 | 1.137 |
| Largest difference peak and hole (e Å ⁻³) | 1.701 and -1.370 | 2.640 and -1.168 | 0.479 and -0.762 |